



Electrophoretic deposition of chitosan–bioglass[®]–hydroxyapatite–halloysite nanotube composite coating

Arman Molaei, MardAli Yousefpour* 

Received: 29 April 2017/Revised: 5 September 2017/Accepted: 5 March 2018/Published online: 5 April 2018
© The Nonferrous Metals Society of China and Springer-Verlag GmbH Germany, part of Springer Nature 2018

Abstract The composite coatings of chitosan (CS)–bioglass[®] (BG)–hydroxyapatite (HA)–halloysite nanotube (HNT) were investigated and produced via electrophoretic deposition (EPD) technique. The utilization of CS as a dispersing, blending and charging agent for ceramic particles, including BG, HA and HNT, allowed the formation of CS–BG/HA/HNT composite, functionally graded composite (FGC) and bilayer film containing different layers. The results of scanning electron microscopy (SEM), energy-dispersive spectrometry (EDS), X-ray diffraction (XRD) and Fourier transform infrared spectroscopy (FTIR) illustrate the composite in the form of the optimum distribution of ceramic components in the CS matrix with thickness of 28 μm on titanium (Ti) substrate. Electrochemical impedance spectroscopy (EIS) and potentiodynamic polarization tests indicate that the corrosion resistance of the coated sample increases in corrected simulated body fluid (C-SBF) at 37 °C. Finally, the apatite-inducing ability of CS–BG–HA–HNT is proved by the formation of carbonated hydroxyapatite particles on composite coating in C-SBF.

Keywords Four-component coating; Composites; Biomaterials; Electrophoretic deposition; Corrosion

1 Introduction

The developed prostheses in the different categories of composite, implant and scaffold are obtained by exploiting sciences in medical, material and surface engineering [1]. Owing to low osteoinductive properties, low tissue would form on metallic implant like titanium and its alloys, and stainless steel [2]. Therefore, surface engineering has been utilized to modify the surface of living replacement [3]. Surface engineering has introduced diverse methods such as dip coating, layer by layer, electrophoretic deposition (EPD) to induce biomedical properties in the orthopedic implants [3–7]. Indeed, EPD technique has been used because of its desirable characteristics consisting of simplicity, deposition on the substrates with complex figure and complex layer formation. EPD consists of two processes: the movement of charged powder particles suspended in a liquid under an applied electric field between two electrodes (electrophoresis), followed by the deposition of these particles on one of the electrodes (deposition) [8].

It has been proved that the appropriate design of composite coating in the form of ceramics embedded in chitosan (CS) matrix causes high-temperature processing elimination, the smooth dispersion of ceramic particles, superior adhesion and optimum ionic release rate [9]. These synthetic materials have desirable applications in tissue engineering such as biosensor, implant, composite and scaffold [3, 9–12]. Chitosan is a well-known polycationic polymer that has one amino group and two hydroxyl groups in the repeating glucosidal residue. In the recent studies, chitosan has been used for the improvement of biocompatibility, biodegradability, bioadhesion and drug delivery [13].

A. Molaei
Department of Materials Engineering, Tehran Science and Research Branch, Islamic Azad University, Tehran 1477893855, Iran

M. Yousefpour*
Faculty of Materials Science and Metallurgical Engineering, Semnan University, Semnan 3513119111, Iran
e-mail: myousefpour@semnan.ac.ir

Owing to high-grade biocompatibility and controllable properties, numerous bioceramics such as bioglass (BG), hydroxyapatite (HA) and halloysite nanotube (HNT) have been introduced. The well-known bioactivity of bioglass[®] and the desirable biocompatibility of hydroxyapatite cause a great interest in applying on metallic implants [14–17]. There are different techniques that have been used to produce BG and HA coatings on metallic substrates [18–22]. However, the weak mechanical properties of these compositions, particularly low adhesion, strength and wear resistance, have hindered their applications as coatings on the biomedical implants. Halloysite nanotube (HNT) is a natural clay mineral with nanotubular layered structure [23, 24]. Applicable properties such as biodegradability, superdispersion and sustained release rate [24, 25] introduce HNT as a favorable nanomaterial used in a broad range of biological applications like thin-film biosensors [25, 26], biocomposites [23] and protective coatings [27, 28].

The EPD of biomaterial was introduced with a mono-component coating of HA in 1986, and then Zhitomirsky and Hashambhoy [29] and Krause et al. [30] developed the coatings of chitosan and BG, respectively. In order to develop EPD process for the introduction of the composites with ameliorated properties and suitable applications, Zhitomirsky et al. investigated EPD of co-deposition of CS–HA, CS–BG and CS–HNT, respectively [31–34]. Moreover, three-component composites of CS–BG–HA [33] and CS–HA–HNT [34] were deposited. In spite of the improved properties, these composites have not compromised a wide range of applications from implant, scaffold, drug delivery system and biosensor to supporting coatings. Therefore, scientists have attempted to design a prosthesis with various properties and broad range of applications.

In the presented research, the first coating consisting of four-component of chitosan, bioglass[®], hydroxyapatite and halloysite nanotube was fabricated and investigated by EPD technique on titanium substrate. Also, morphological, structural, corrosion resistance and apatite-inducing ability were analyzed to check composite coating. It can be expected that this composite presents broad properties during implantation.

2 Experimental

2.1 Materials and suspension preparation

Medium molecular weight chitosan ($MW = 80 \text{ kg}\cdot\text{mol}^{-1}$) with a degree of deacetylation (DD) of about 85%, acetic acid (> 98%), ethanol, SiO_2 , Na_2CO_3 , CaCO_3 , $\text{Ca}(\text{NO}_3)_2\cdot 4\text{H}_2\text{O}$ and P_2O_5 was purchased from Sigma-Aldrich. Dilute chitosan solution was prepared by

dissolving $0.5 \text{ g}\cdot\text{L}^{-1}$ chitosan in 1% acetic acid solution and stirring at room temperature for 24 h. Bioglass[®] was produced by a melting technique [35]. To obtain a sub-micron powder in the size range up to $37 \mu\text{m}$, as-synthesized bioactive glass was dried and sieved. Hydroxyapatite nanoparticles were prepared by a sol–gel method [22]. HNT with chemical formula of $\text{Al}_2\text{Si}_2\text{O}_5(\text{OH})_4\cdot 2 \text{H}_2\text{O}$ and MW of $294.19 \text{ kg}\cdot\text{mol}^{-1}$ was purchased from Sigma-Aldrich.

EPD was performed from $0.5 \text{ g}\cdot\text{L}^{-1}$ CS solutions in a mixed ethanol–30 vol% water solvent containing $0\text{--}1 \text{ g}\cdot\text{L}^{-1}$ BG, $0\text{--}0.7 \text{ g}\cdot\text{L}^{-1}$ HA and $0\text{--}0.6 \text{ g}\cdot\text{L}^{-1}$ HNT at $\text{pH} = 2.8$. The optimum concentrations of components in their composites were taken from Refs. [17, 20, 22, 34]. The suspension was sonicated for 20 min after stirring by a magnetic stirrer for 120 min in order to break down the agglomerates. The deposition was performed at a constant voltage in the range of 10–30 V, and the deposition time was varied in the range of 1–15 min.

Thus, the EPD cell includes titanium ($1 \text{ mm}\times 20 \text{ mm}\times 35 \text{ mm}$) and 316L stainless steel ($1 \text{ mm}\times 21 \text{ mm}\times 37 \text{ mm}$) plates as cathode and anode electrodes, respectively. A constant distance of 15 mm was designed between electrodes. The surface of electrode was polished by SiC abrasive papers and then rinsed with deionized water and ethanol in an ultrasonic bath. In case of titanium, the electrode was etched in a solution containing HF and HNO_3 for 10 s and rapidly rinsed in ethanol and dried.

2.2 Characterization

The morphology and the cross section of coatings were analyzed by scanning electron microscope (SEM, JXA—840, JEOL). The quantitative elemental analysis was studied by energy-dispersive spectrometry (EDS, Oxford Instruments). The thickness of composite was measured by coating thickness gauge (Electrometer 456), and the medium value was presented. The crystal structures of coatings were assigned via X-ray diffractometer (XRD, 3003 PTS, Seifert) with Cu $K\alpha$ radiation ($\lambda = 0.154 \text{ nm}$) using the 2θ range of $10^\circ\text{--}80^\circ$ with a step size of 0.04° and a count rate of 50 s per step.

Fourier transform infrared spectroscopy (FTIR, Nexus 870, Thermo-Nicolet) was used to characterize intermolecular bindings between the components of coating in the wavenumber of $4000\text{--}400 \text{ cm}^{-1}$. To investigate the corrosion behavior of the uncoated and coated samples, polarization test and electrochemical impedance spectroscopy (EG & G model 273 A) were carried out in corrected simulated body fluid (C-SBF) at 37°C . C-SBF solution was prepared according to the procedure described by Kokubo et al. [35]. The counter and the reference

electrodes were platinum plate and standard calomel electrode (SCE), respectively. The surface area of the working electrode was 1 cm^2 . The impedance spectra were acquired in the frequency range of 0.1 mHz to 0.1 MHz with a 5 mV amplitude.

In order to explore apatite-inducing ability of composite-coated samples, the SBF test was performed. The SBF was prepared according to Kokubo's method, with the concentration of ions nearly equal to those of the human blood plasma [36]. The coated samples ($10.0 \text{ mm} \times 10.0 \text{ mm} \times 0.2 \text{ mm}$) were immersed in 50 ml SBF and then were incubated at $37 \text{ }^\circ\text{C}$ for 22 days. The sample was removed from SBF, rinsed with deionized water, left to dry in incubator and then stored in desiccators. Carbonated hydroxyapatite deposition formed on the coatings was analyzed by FESEM/EDX.

3 Results and discussion

3.1 Morphological characterization

The suspensions of HNT are unstable and show fast sedimentation. No EPD is achieved from such suspensions. The addition of CS results in ameliorating suspension stability. The cathodic macromolecules of CS act as interconnection among the ceramic particles under the van der Waals forces and result in improving the distribution of particles and allowing the formation of cathodic depositions [20].

Figure 1 illustrates the morphology of composite film with $0.5 \text{ g}\cdot\text{L}^{-1}$ CS and $0.6 \text{ g}\cdot\text{L}^{-1}$ HNT. As seen in Fig. 1, no agglomeration of HNTs is formed in composite. Desirable homogeneity and integrity are obvious in CS–HNT film with the thickness of approximately $5 \text{ }\mu\text{m}$.

Figure 2a, b shows morphologies of three- and four-component films with $0.5 \text{ g}\cdot\text{L}^{-1}$ CS, $1.0 \text{ g}\cdot\text{L}^{-1}$ BG and $0.4 \text{ g}\cdot\text{L}^{-1}$ HA and $0.5 \text{ g}\cdot\text{L}^{-1}$ CS, $1 \text{ g}\cdot\text{L}^{-1}$ BG, $0.4 \text{ g}\cdot\text{L}^{-1}$ HA and $0.6 \text{ g}\cdot\text{L}^{-1}$ HNT, respectively. Clusters with high

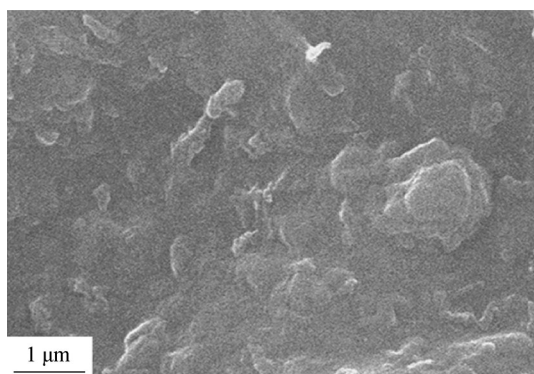


Fig. 1 SEM image of CS–HNT composite films prepared from $0.5 \text{ g}\cdot\text{L}^{-1}$ CS solution containing $0.6 \text{ g}\cdot\text{L}^{-1}$ HNT

amount of BG and low amount of HA attached to each other by CS polymer form on Ti (Fig. 2a). There is a significant difference between BG and HA depositions in composite. The high concentration and the large size of BG in the suspension result in the high amount of this component in composite film. Figure 2b presents four-component composite film with high BG deposition on the substrate. The EDS results display high peak of Si relating to BG and HNT and small peak of Al relating to HNT. It is approved that BG with high amount is embedded in composite (Fig. 2c).

Zeta potential of BG is significantly higher than that of HA in suspension [20]. Particles with higher Zeta potential have more mobility of moving faster toward the electrode with opposite electric charge. Therefore, BG has more deposition than HA on Ti substrate. It is demonstrable that heterogeneous CS–BG–HA–HNT composite with high BG concentration and low HA concentration is reached (Fig. 2). Therefore, the goal is to obtain optimum quantities of both BG and HA particles in the CS-based composite film. The optimum and uniform multicomponent film can be yielded by a variety of method including utilizing additives, changing EPD parameters and modifying component concentration in suspension [21, 31, 32, 34].

Figure 3a, b depicts the surface morphology of four-component composite film with $0.5 \text{ g}\cdot\text{L}^{-1}$ CS, $0.7 \text{ g}\cdot\text{L}^{-1}$ BG, $0.7 \text{ g}\cdot\text{L}^{-1}$ HA and $0.6 \text{ g}\cdot\text{L}^{-1}$ HNT in different magnifications. Arrows show four constituent particles in composite (Fig. 3a). It is observable that four components uniformly deposit on Ti substrate by changing components concentration in suspension. SEM image and EDS analyses confirm that the suitable distribution of components with approximately balanced HA and BG particles is obtained by decreasing BG concentration down to $0.7 \text{ g}\cdot\text{L}^{-1}$ and increasing HA concentration up to $0.7 \text{ g}\cdot\text{L}^{-1}$ in suspension (Fig. 3b, c). The optimum film with the uniform presences of components is yielded. The reason for this behavior is the change of components' concentrations in suspension (Figs. 2, 3).

3.2 Mechanism of chitosan-based coating

The mechanism of electrophoretic deposition of chitosan along with other particles has been represented in Ref. [13]. Applied electrical field and yield positive charges lead to the electrophoresis of embedded particles into the suspension. Then, CS hydrophobic macromolecular chains with amino groups bonded to ceramic particles move toward cathode electrode under the influence of applied electrical field. As illustrated in Fig. 4, a distinguished mechanism for the deposition of ceramic particles in the CS matrix relates to the preassembling of HNT and nano-HA particles chelated by CS. Then, due to CS macromolecules, these

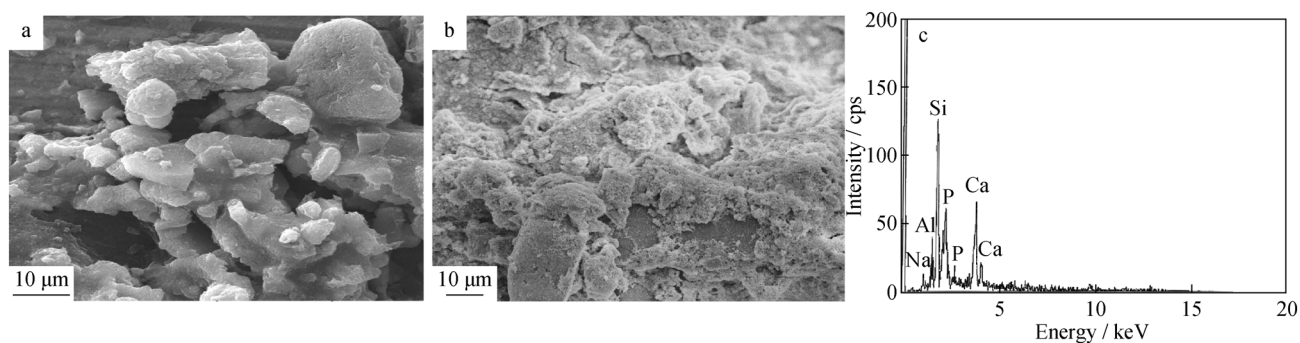


Fig. 2 SEM images of **a** CS–BG–HA and **b** CS–BG–HA–HNT composite films and **c** EDS analysis of CS–BG–HA–HNT

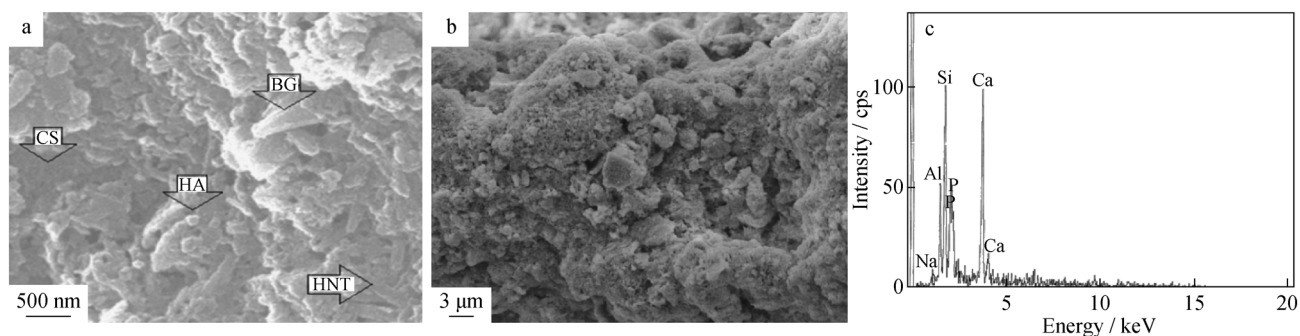


Fig. 3 SEM images of CS–BG–HA–HNT composite films: **a** high magnification (arrows showing constituent particles) and **b** low magnification; **c** EDS analysis of CS–BG–HA–HNT

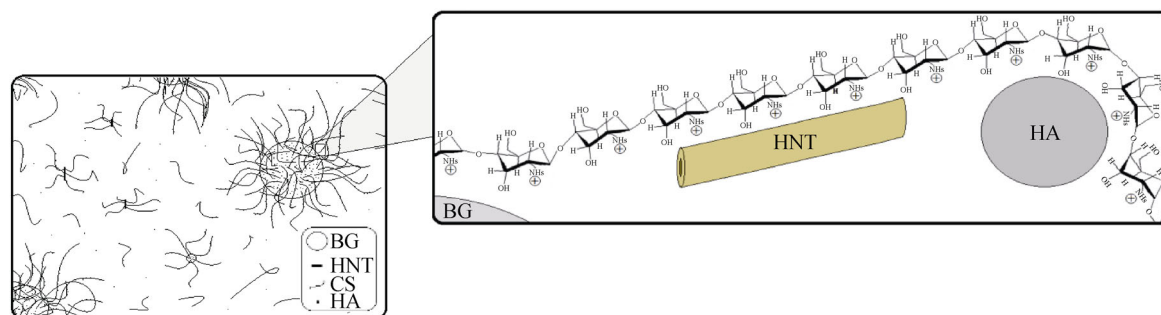


Fig. 4 Schematic view of EPD mechanism of CS–BG–HA–HNT

agglomerations deposit on BG microparticles. This mechanism complies well with Fig. 2b. The steric stabilization mechanism establishes in suspension under the repulsive forces between CS macromolecular chains that are joined to ceramic particles. Consequently, they deposit under the influence of an applied voltage on Ti electrode.

3.3 Deposition of cross section, bilayer and functionally graded film

Figure 5a shows a cross section of a CS-based composite film. The thicknesses of uniform deposits are approximately 28 μm. The chitosan acts as a binding bond between ceramic particles and substrate which enhances

deposition's cohesion [20, 21]. Cross section of a CS–HNT/CS–BG–HA bilayer film is displayed in Fig. 5b. At the upper layer, agglomerations with the presence of BG in the center and CS, HA and HNT around BG are obvious. The top layer containing HA provides a bioactive surface for composite coatings. The CS–HNT layer can be used for the controlled release of drugs or antimicrobial agents. Moreover, the release rate of various species from the CS–HNT layer can be modified by the change of the thickness and composition of the top layer [22].

Figure 5c indicates a cross section of a functionally graded composite film containing pure CS layer, composite CS–HNT and CS–BG–HA layer. The formation of CS film at the interface between composite film and titanium

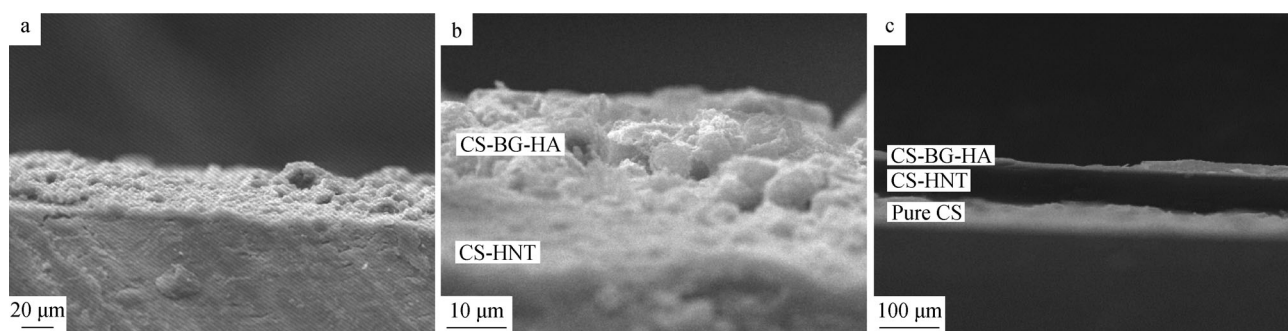


Fig. 5 SEM image of a cross section for **a** composite film prepared from $0.5 \text{ g}\cdot\text{L}^{-1}$ CS solutions containing $0.7 \text{ g}\cdot\text{L}^{-1}$ BG, $0.7 \text{ g}\cdot\text{L}^{-1}$ HA and $0.6 \text{ g}\cdot\text{L}^{-1}$ HNT, **b** bilayer film containing layers prepared from $0.5 \text{ g}\cdot\text{L}^{-1}$ CS solutions containing $0.6 \text{ g}\cdot\text{L}^{-1}$ HNT, $0.7 \text{ g}\cdot\text{L}^{-1}$ BG and $0.7 \text{ g}\cdot\text{L}^{-1}$ HA and **c** composite film of graded composition, containing layers, prepared from $0.5 \text{ g}\cdot\text{L}^{-1}$ chitosan solutions containing $0.7 \text{ g}\cdot\text{L}^{-1}$ BG, $0.7 \text{ g}\cdot\text{L}^{-1}$ HA and $0.6 \text{ g}\cdot\text{L}^{-1}$ HNT

provides high coating-to-substrate adhesion. HNTs embedded in CS polymer ameliorate drug delivery properties. Also, the CS–BG–HA layer provides suitable biocompatibility and bioactivity, as well as good interfacial bonding to tissue. Therefore, further studies are necessary for the investigation of properties of multilayer and functionally graded coatings containing CS, BG, HA and HNT particles prepared by EPD.

3.4 XRD and FTIR analysis

The diffraction patterns of composite films deposited on titanium substrate are shown in Fig. 6a. The studied peaks of CS–HNT and CS–BG–HA are exactly repeated in those of CS–BG–HA–HNT. The diffraction peaks of HNT and HA are identified from CS–HNT and CS–BG–HA, respectively (JCPDS No. 9-0432 for HA and JCPDS No. 29-1489 for HNT). The analyzed Ti peaks are originated from Ti substrate (JCPDS No. 44-1294 for Ti). CS and BG depositions are in the form of semicrystalline and amorphous, respectively.

Figure 6b illustrates FTIR spectra of multicomponent films. The studied FTIR peaks of CS–HNT and CS–BG–HA are exactly repeated in those of CS–BG–HA–HNT. The peak around 466 cm^{-1} is due to the stretching modes of Si–O–Si and P–O bonds. 568 cm^{-1} is related to the bending bonds of Si–O–Si, Al–O–Si and P–O [20]. C–O has stretching mode at 760 and 870 cm^{-1} . The wavenumber at 915 cm^{-1} is pertained to the stretching bonds of Si–O–Si and C–O. The bonds near 1020 – 1070 cm^{-1} are belonged to CO of the ring COH, COC and CH_2OH and also in-plane Si–O stretching of HNTs, as well as P–O bond [22]. The bonds at 1420 and 2927 cm^{-1} show the symmetric stretching bond of C–H in CH_2 and CH_3 . Peaks at 1484 , 2356 and 3427 cm^{-1} are related to hydroxyl groups and CO_2 that are adsorbed from the atmosphere, respectively. The intercalated water of HNT and also adsorbed water are related to 3448 cm^{-1} . The presence of the hydroxyl groups of HNT particles is assigned at 3628 and 3688 cm^{-1} , relating to Al_2OH stretching bond and also the stretching bond of Si–O–Si and P–O bond [34].

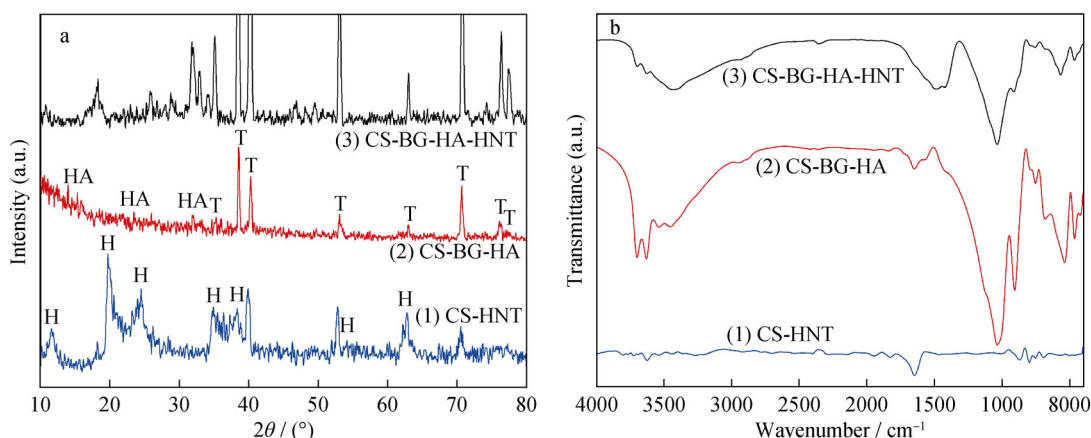


Fig. 6 **a** XRD patterns and **b** FTIR spectra of films prepared from $0.5 \text{ g}\cdot\text{L}^{-1}$ CS solutions containing (1) $0.6 \text{ g}\cdot\text{L}^{-1}$ HNT, (2) $0.7 \text{ g}\cdot\text{L}^{-1}$ BG, $0.7 \text{ g}\cdot\text{L}^{-1}$ HA and (3) $0.7 \text{ g}\cdot\text{L}^{-1}$ BG, $0.7 \text{ g}\cdot\text{L}^{-1}$ HA and $0.6 \text{ g}\cdot\text{L}^{-1}$ HNT

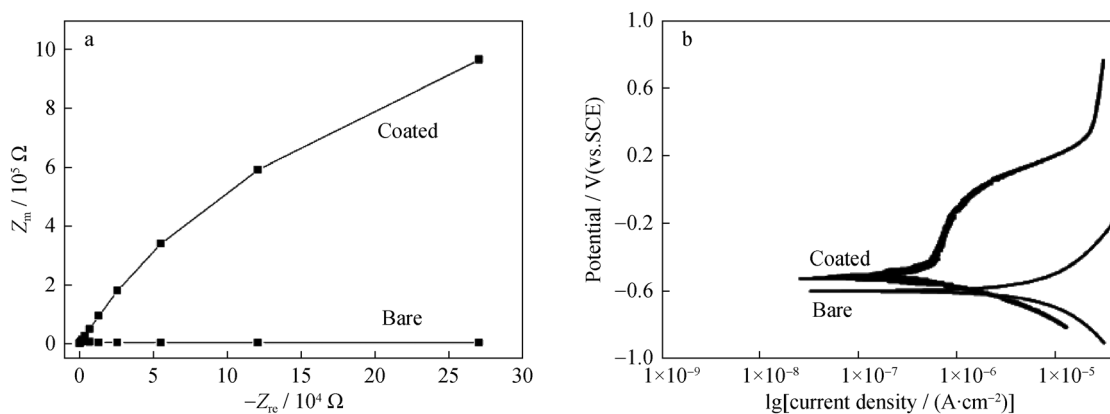


Fig. 7 **a** EIS data in Nyquist plot (Z_{in} is the imaginary impedancem and Z_{re} is the real impedance) and **b** polarization curves of bare and CS–BG–HA–HNT-coated samples prepared from $0.5 \text{ g}\cdot\text{L}^{-1}$ CS solution containing $0.7 \text{ g}\cdot\text{L}^{-1}$ BG, $0.7 \text{ g}\cdot\text{L}^{-1}$ HA and $0.6 \text{ g}\cdot\text{L}^{-1}$ HNT in C-SBF at 37°C

Table 1 I_{corr} and E_{corr} for bare Ti and coated sample prepared from $0.5 \text{ g}\cdot\text{L}^{-1}$ CS solution containing $0.7 \text{ g}\cdot\text{L}^{-1}$ BG, $0.7 \text{ g}\cdot\text{L}^{-1}$ HA and $0.6 \text{ g}\cdot\text{L}^{-1}$ HNT in C-SBF at 37°C

Samples	E_{corr}/V	$I_{corr}/(\mu\text{A}\cdot\text{cm}^{-2})$
Bare Ti	− 0.61	10.5
Coated Ti	− 0.51	0.578

3.5 Impedance spectroscopy and electrochemical polarization studies

Figure 7a shows the impedance spectra measured at open-circuit potential for uncoated and coated samples exposed to C-SBF at 37°C . Although bare sample depicts a low amount of impedance, the coated sample shows the expected passive behavior in the neutral solution with high amounts of impedance and suggests a higher corrosion resistance. The quarter circular spectrum of the coated sample is observed in Fig. 7a. The reason for this behavior is a high surface roughness of deposition and the lack of

physical uniformity of deposited particles [36]. Figure 7b displays the polarization curves of uncoated and coated samples recorded in C-SBF solution at 37°C . The amounts of corrosion potential and corrosion current density are listed in Table 1. The current density of the uncoated sample is 18 times more than that of the coated one. Polarization test depicts that the four-component coating decreases the corrosion current density of Ti substrate. Electrochemical impedance and potentiodynamic polarization indicate that four-component coating acts as a barrier and prevents the diffusion of corrosive ions and consequently the corrosion of substrate.

3.6 Growth of carbonated hydroxyapatite on composite coating

The new nanostructured phase is formed on the surface of CS–BG–HA–HNT composite after a few immersion days in SBF solution (Fig. 8a). SEM image and EDS spectrum of CS–BG–HA–HNT composites after immersion in SBF solution confirm that the new phase has more amounts of

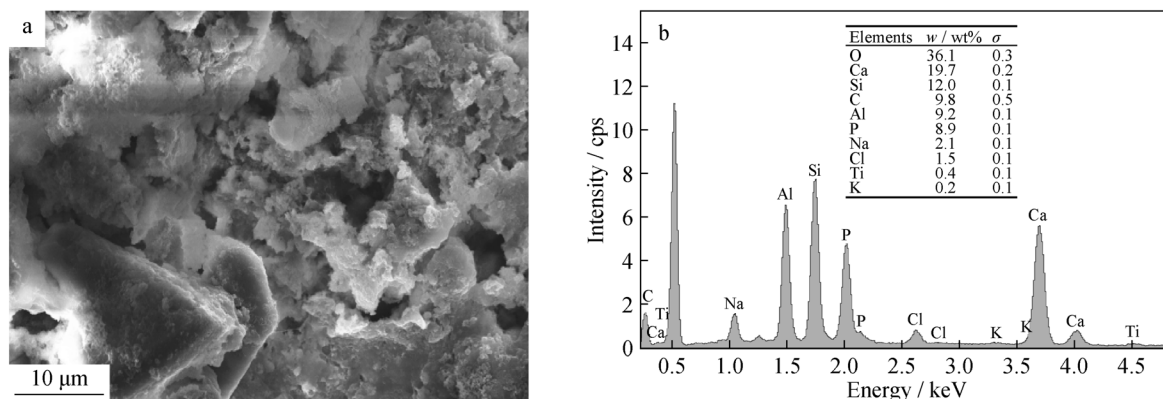


Fig. 8 **a** SEM images and **b** EDS analyses of CS–BG–HA–HNT composites prepared from $0.5 \text{ g}\cdot\text{L}^{-1}$ CS solution containing $0.7 \text{ g}\cdot\text{L}^{-1}$ BG, $0.7 \text{ g}\cdot\text{L}^{-1}$ HA and $0.6 \text{ g}\cdot\text{L}^{-1}$ HNT immersion in SBF solution after 14 days (σ , standard deviation)

Ca and P atoms. This result reveals that deposited particles are carbonated hydroxyapatite (Fig. 8a, b). The carbonated hydroxyapatite deposited places are covered with osteoblastic cells in body. The reason for this behavior relates to osteocalcin proteins which are important non-collagen proteins in bone. The osteoconductive composites enhance the bone-forming ability and rapid bone interaction of metallic implants due to an improved initial osseointegration rate [35].

4 Conclusion

The electrophoretic deposition of CS–BG–HA–HNT was successfully preassembled and deposited on titanium substrate. The depositions with the smooth distribution of ceramic particles in the CS matrix were yielded. The uniform composite coatings with desirable structure and bonding that are formed among micro- and nanoparticles were fabricated. The main mechanism of composite coating formation is preassembled HNT and nano-HA particles chelated by CS on BG microparticle. The formation of CS–BG–HA–HNT monolayer, functionally graded composite and bilayer film containing different layers are acquired. The four-component deposition improves the corrosion resistance of titanium substrate in C-SBF solution. Also, the formation of carbonated hydroxyapatite on CS–BG–HA–HNT shows the apatite-inducing ability of coating. This research will be introduced for producing composites with multiple properties and different applications.

References

- [1] Sun F, Zhou H, Lee J. Various preparation methods of highly porous hydroxyapatite/polymer nanoscale biocomposites for bone regeneration. *Acta Biomater.* 2011;7(11):3813.
- [2] Lian Z, Guan H, Ivanovski S, Loo YC, Johnson NW, Zhang H. Effect of bone to implant contact percentage on bone remodelling surrounding a dental implant. *Int J Oral Maxillofac Surg.* 2010;39(7):690.
- [3] Caridade SG, Merino EG, Alves NM, Mano JF. Biomineralization in chitosan/Bioglass® composite membranes under different dynamic mechanical conditions. *Mater Sci Eng C.* 2013;33(7):4480.
- [4] Abdal-hay A, Barakat N, Kyoo Lim J. Influence of electrospinning and dip-coating techniques on the degradation and cytocompatibility of Mg-based alloy. *Colloids Surf A Physicochem Eng Asp.* 2013;420:37.
- [5] Pinheiro AC, Bourbon AI, Quintas MAC, Coimbra MA, Vicente AA. K-carrageenan/chitosan nanolayered coating for controlled release of a model bioactive compound. *Innov Food Sci Emerg Technol.* 2012;16:227.
- [6] Wang Y, Pang X, Zhitomirsky I. Electrophoretic deposition of chiral polymers and composites. *Colloids Surf B Biointerfaces.* 2011;87(2):505.
- [7] Li Y, Wu K, Zhitomirsky I. Electrodeposition of composite zinc oxide–chitosan films. *Colloids Surf A Physicochem Eng Asp.* 2010;356(1):63.
- [8] Laxmidhar B, Meilin L. A review on fundamentals and applications of electrophoretic deposition (EPD). *Prog Mater Sci.* 2007;52(1):1.
- [9] Simchi A, Tamjid E, Pishbin F, Boccaccini AR. Recent progress in inorganic and composite coatings with bactericidal capability for orthopaedic applications. *Nanomedicine.* 2011;7(1):22.
- [10] Liang D, Lu Zh, Yang H, Gao J, Chen R. Novel asymmetric wettable AgNPs/chitosan wound dressing: in vitro and in vivo evaluation. *ACS Appl Mater Interfaces.* 2016;8(2):3958.
- [11] Lu Z, Gao J, He Q, Wu J, Liang D, Yang H, Chen R. Enhanced antibacterial and wound healing activities of microporous chitosan–Ag/ZnO composite dressing. *Carbohydr Polym.* 2017;156:460.
- [12] Su CH, Yang H, Song Sh, Lu B, Chen R. A magnetic superhydrophilic/oleophobic sponge for continuous oil–water separation. *Chem Eng J.* 2017;309:366.
- [13] George M, Abraham TE. Polyionic hydrocolloids for the intestinal delivery of protein drugs: alginate and chitosan—a review. *J Control Release.* 2006;114(1):1.
- [14] Hench LL. The story of bioglass. *J Mater Sci Mater Med.* 2006;17(11):967.
- [15] Batmanghelich F, Ghorbani M. Effect of pH and carbon nanotube content on the corrosion behavior of electrophoretically deposited chitosan–hydroxyapatite–carbon nanotube composite coatings. *Ceram Int.* 2013;5(5):5393.
- [16] Fu C, Song B, Wan CH, Savino K, Wang Y, Zhang X, Yates MZ. Electrochemical growth of composite hydroxyapatite coatings for controlled release. *Surf Coat Technol.* 2015;276:618.
- [17] Fu C, Zhang X, Savino K, Gabrys P, Gao Y, Chaimayo W, Miller BL, Yates MZ. Antimicrobial silver–hydroxyapatite composite coatings through two-stage electrochemical synthesis. *Surf Coat Technol.* 2016;301:13.
- [18] Krause D, Thomas B, Leinenbachb Ch, Eifler D, Minaya EJ, Boccaccini AR. The electrophoretic deposition of Bioglass® particles on stainless steel and Nitinol substrates. *Surf Coat Technol.* 2006;200(16):4835.
- [19] Mirsalehi SA, Sattari M, Khavandi A, Mirdamadi S, Naimi-Jamal MR. Tensile and biocompatibility properties of synthesized nano-hydroxyapatite reinforced ultrahigh molecular weight polyethylene nanocomposite. *J Compos Mater.* 2015;13:1.
- [20] Molaei A, Amadeh A, Yari M, Afshar MR. Structure, apatite inducing ability, and corrosion behavior of chitosan/halloysite nanotube coatings prepared by electrophoretic deposition on titanium substrate. *Mater Sci Eng C.* 2016;59:740.
- [21] Mirsalehi SA, Khavandi A, Mirdamadi S, Naimi-Jamal MR, Kalantari SM. Nanomechanical and tribological behavior of hydroxyapatite reinforced ultrahigh molecular weight polyethylene nanocomposites for biomedical applications. *J Appl Polym Sci.* 2015;132(23):42052.
- [22] Molaei A, Yari M, Afshar MR. Modification of electrophoretic deposition of chitosan-bioactive glass-hydroxyapatite nanocomposite coatings for orthopedic applications by changing voltage and deposition time. *Ceram Int.* 2015;41(10):14537.
- [23] Deen I, Zhitomirsky I. Electrophoretic deposition of composite halloysite nanotube–hydroxyapatite–hyaluronic acid films. *J Alloy Compd.* 2014;586:531.
- [24] Vergaro V, Abdullayev E, Lvov YM, Zeitoun A, Cingolani R, Rinaldi R, Leporatti S. Cytocompatibility and uptake of halloysite clay nanotubes. *Biomacromol.* 2010;11(3):820.
- [25] Zhang Y, Chen Y, Zhang H, Zhang B, Liu J. Potent antibacterial activity of a novel silver nanoparticle-halloysite nanotube nanocomposite powder. *J Inorg Biochem.* 2013;118:59.

- [26] Sun X, Zhang Y, Shen H, Jia N. Direct electrochemistry and electrocatalysis of horseradish peroxidase based on halloysite nanotubes/chitosan nanocomposite film. *Electrochim Acta*. 2010;56(2):700.
- [27] Kamble R, Ghag M, Gaikawad S, Panda BK. Halloysite nanotubes and applications: a review. *J Adv Sci Res*. 2012;3(2):25.
- [28] Ducheyne P, Van Raemdonck W, Heughebaert JC, Heughebaert M. Structural analysis of hydroxyapatite coatings on titanium. *Biomaterials*. 1986;7(2):97.
- [29] Zhitomirsky I, Hashambhoy A. Chitosan-mediated electrosynthesis of organic–inorganic nanocomposites. *J Mater Process Technol*. 2007;191(1):68.
- [30] Buhl S, Leinenbach C, Spolenak R, Wegener K. Influence of the brazing parameters on microstructure, residual stresses and shear strength of diamond-metal joints. *J Mater Sci*. 2010;45(16):4358.
- [31] Pang X, Zhitomirsky I. Electrophoretic deposition of composite hydroxyapatite–chitosan coatings. *Mater Charact*. 2007;58(4):339.
- [32] Zhitomirsky D, Roether JA, Boccaccini AR, Zhitomirsky I. Electrophoretic deposition of bioactive glass/polymer composite coatings with and without HA nanoparticle inclusions for biomedical applications. *J Mater Process Technol*. 2009;209(4):1853.
- [33] Deen I, Pang X, Zhitomirsky I. Electrophoretic deposition of composite chitosan–halloysite nanotube–hydroxyapatite films. *Colloids Surf A*. 2012;410:38.
- [34] Naghib SM, Ansari M, Pedram A, Moztarzadeh F, Feizpour A, Mozafari M. Bioactivation of 304 stainless steel surface through 45S5 bioglass coating for biomedical applications. *Int J Electrochem Sci*. 2012;7:2890.
- [35] Kokubo T, Takadama H. How useful is SBF in predicting in vivo bone bioactivity? *Biomaterials*. 2006;27(15):2907.
- [36] Ehteshamzadeh M. Introduction to application of EIS in corrosion study, vol. 29. 1st ed. Kerman: Shahid Bahonar University Press; 2007, 19.